High-spin spectroscopy of ^{144}Tb: Systematic investigation of dipole bands in $N = 79$ isotones

Y. Y. Cheng, S. Q. Zhang, X. Q. Li,* H. Hua,† C. Xu, Z. H. Li, P. W. Zhao, J. Meng, J. J. Sun, Z. J. Bai, F. R. Xu, Y. L. Ye, D. X. Jiang, E. H. Wang, C. He, and R. Han

School of Physics and State Key Laboratory of Nuclear Physics and Technology, Peking University, Beijing 100871, China

X. G. Wu, G. S. Li, C. Y. He, Y. Zheng, C. B. Li, S. P. Hu, S. H. Yao, B. B. Yu, X. P. Cao, and J. L. Wang

China Institute of Atomic Energy, Beijing 102413, China

(Received 30 December 2013; revised manuscript received 6 March 2014; published 8 May 2014)

The high-spin spectroscopy of ^{144}Tb has been studied via ^{116}Sn(^{32}S, $3n1p$)^{144}Tb fusion-evaporation reaction at a beam energy of 156 MeV. A dipole band built on the $\pi h_{11/2}^3 \otimes \nu h_{11/2}^{-1}$ configuration is newly observed in ^{144}Tb. Together with similar observation in neighboring nuclei, the properties of dipole bands in $N = 79$ isotones are investigated in terms of the self-consistent tilted-axis-cranking covariant density functional theory. Based on systematic comparison and examination of the shears mechanism, the dipole band in ^{144}Tb can be interpreted as a magnetic rotational band.

DOI: 10.1103/PhysRevC.89.054309 PACS number(s): 21.10.Re, 23.20.Lv, 25.70.Gh, 27.60.+j

I. INTRODUCTION

The light rare-earth nuclei with $77 < N < 82$, $Z \sim 64$ are situated in the transitional region between the closed-shell (spherical) $N = 82$ nuclei and the well deformed mass region with $N \leqslant 77$. Due to the competition of the collective vibrational, rotational, and single-particle degrees of freedom, the level schemes in these transitional nuclei have complex structures. Thus, spectroscopic studies of these transitional nuclei provide a good opportunity to test the predictions of different theoretical models and have drawn considerable attention in the recent past.

For the $N = 79$ odd-odd nuclei ^{138}Pr, ^{140}Pm, ^{142}Eu and ^{144}Tb, in addition to the valence nucleons filling the $1g_{7/2}$, $2d_{5/2}$, $3s_{1/2}$, and $2d_{3/2}$ orbitals, both the neutron and proton negative-parity $1h_{11/2}$ orbitals are also close to the Fermi surface. They play an important role in the level structures of these nuclei and result in low-lying high-spin negative-parity isomers, which have been experimentally identified and in many cases will undergo direct β decay [1–7]. Above these isomers, the positive-parity level schemes in these isotones show an interesting transition from collective to single-particle structure between $Z = 61$ and 63. The low-energy parts of positive-parity states with spins ranging from 8^+ to 11^+ in these isotones have been proposed to be built predominantly on the $\pi h_{11/2} \otimes \nu h_{11/2}^{-1}$ configuration [1–4]. For the lighter $N = 79$ isotones ^{138}Pr and ^{140}Pm, collective rotational bands built on this $\pi h_{11/2} \otimes \nu h_{11/2}^{-1}$ configuration with modestly β_2 deformation were established [8,9], while, for the heavier $N = 79$ isotone ^{142}Eu with only a proton-hole in the $Z = 64$ subshell closure, the single- and multiparticle excitations were suggested to dominate the low-energy positive-parity yrast levels with essentially spherical shape [3,10]. In addition to the spherical parts of the level schemes, a rotation-like positive-parity sequence has also been observed in ^{142}Eu [10]. Total Routhian surface (TRS) calculations show that this collective band structure may have triaxial shape ($\beta_2 \sim 0.12$, $\gamma \sim 30^\circ$) [10] and present evidence for shape coexistence in this transitional nucleus.

For the ^{144}Tb with one proton-particle outside $Z = 64$ subshell closure, the level structures have been previously studied up to 5 MeV excitation via in-beam γ-ray spectroscopy and the low excitation energy parts of the level schemes have been well described with the spherical shell model [4,11], indicating a predominantly spherical nuclear shape at low excitation energy region. As the excitation energy and spin increase, much more complex nuclear structures show up that cannot be explained by the shell model [11]. To better understand the nature of the high-spin structure and investigate the structure evolution as a function of excitation energy and spin in ^{144}Tb, further spectroscopic study of ^{144}Tb is needed.

Of particular interest in the $Z \sim 64$, $N \sim 82$ mass region is magnetic rotation [12] with the availability of proton particles and neutron holes in high-j $h_{11/2}$ orbitals. Based on the lifetime measurement, the dipole band in ^{139}Sm was the first confirmed magnetic rotational band in this mass region [13]. Later, the dipole bands observed in ^{142,143,144}Gd [14,15], ^{141}Eu [16], ^{146}Tb [17], and ^{144}Dy [18] provided further evidence for magnetic rotation. It is therefore very interesting to search for the possible magnetic rotational band in ^{144}Tb and explore how the magnetic rotation evolves in this mass region. In this work, we present the results of a new investigation of ^{144}Tb. Its level scheme is compared with the similar structures of neighboring nuclei. The newly observed dipole band in ^{144}Tb is discussed in terms of self-consistent tilted-axis-cranking covariant density functional theory (TAC-CDFT) and can be interpreted as a magnetic rotational band.

II. EXPERIMENT AND RESULTS

The present experiment was performed at the HI-13 tandem facility of the China Institute of Atomic Energy. The high-spin states in ^{144}Tb were populated through the ^{116}Sn(^{32}S, $3n1p$)^{144}Tb reaction at a beam energy of 156 MeV. A ^{116}Sn

*Corresponding author: lixq2002@pku.edu.cn
†Corresponding author: hhua@pku.edu.cn

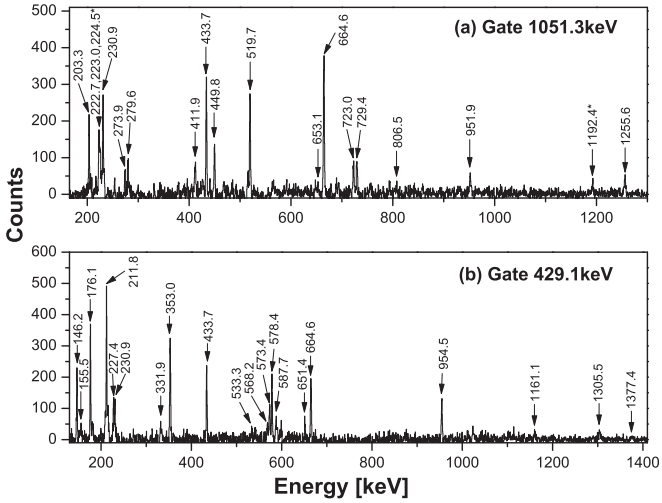

FIG. 1. Coincident γ-ray spectra with gating on (a) 1051.3-keV transition and (b) 429.1-keV transition. The peaks marked with stars are the deexcited transitions from individual levels of ^{144}Tb which do not belong to the established bands.

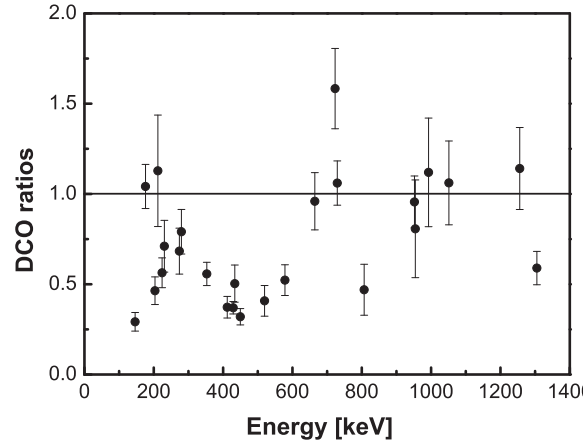

FIG. 2. The DCO ratios as a function of γ-ray energy for transitions in ^{144}Tb.

target with a thickness of 2.3 mg/cm^2 on 14.1 mg/cm^2 Pb backing was used. The deexcitation γ rays were detected by an array of 12 high-purity germanium (HPGe) detectors with bismuth germanate (BGO) anti-Compton suppressors. Two additional planar HPGe detectors were also used to detect low-energy γ rays. The energy resolutions of these detectors were 2.0–3.0 keV at 1.33 MeV. All detectors were calibrated using the standard ^{152}Eu and ^{133}Ba γ-ray sources.

A total of 8.4×10^7 coincident events were collected, from which a symmetric γ-γ matrix was built. The level scheme analysis was performed using the RADWARE software [19]. The typical γ-ray spectra gated on the known γ-ray transitions in ^{144}Tb are shown in Fig. 1. In order to obtain the directional correlations of γ rays deexciting oriented states (DCO) intensity ratios to determine the multipolarities of γ-ray transitions, the detectors around 90° with respect to the beam direction were sorted against the detectors around 40° to produce a two-dimensional angular correlation matrix. To get clean DCO values for transitions in ^{144}Tb, gates were set on uncontaminated stretched $E2$ transitions. In general, stretched quadrupole transitions were adopted if DCO ratios were larger than 1.0, and stretched dipole transitions were assumed if DCO ratios were less than 0.8. The DCO ratio is plotted as a function of γ-ray energy for most of the observed transitions in ^{144}Tb in Fig. 2.

The structure of ^{144}Tb has been previously studied via the ^{112}Sn(^{35}Cl, $n2p$), ^{116}Sn(^{32}S, $3np$) and ^{89}Y(^{58}Ni, $n2p$) fusion-evaporation reactions by Sferrazza *et al.* [4,11]. The level scheme up to $I \sim 20\hbar$ and $E_x \sim 5$ MeV was established. The partial level scheme of ^{144}Tb, deduced from the present work, is shown in Fig. 3. It was constructed from γ-γ coincidence relationships, intensity balances, and DCO analyses. The results are summarized in Table I. The present analysis confirms most of the transitions found in the previous study. The yrast positive-parity band (band 1 in Fig. 3) was extended up to the same level at 5379.5 keV as in Ref. [11]. In Ref. [11], no spins and parities were assigned to the levels at 4664.0 and 5379.5 keV. According to the DCO value obtained in the current work, a quadrupole assignment is made for the transition of 951.9 keV. The γ-ray decay of 715.5 keV for which the DCO ratio could not be extracted is also assumed to be a stretched $E2$ transition.

Band 2 has been established in Ref. [11] and suggested to be possibly based on the $\pi d_{5/2}^{-1} \otimes \nu h_{11/2}^{-1}$ structure coupled to a pair of aligned $h_{11/2}$ protons. In that study, only spins were tentatively assigned to the states in band 2. In the neighboring isotone ^{142}Eu [10], a negative-parity band, which has a decay cascade very similar to band 2 in ^{144}Tb, has been found in almost the same excitation energy range. Here we tentatively take band 2 to have the same negative parity. The present work adds three γ rays of 568.2, 587.7, and 1161.1 keV to the top of band 2.

By requiring coincidence with the known γ-ray transitions under spin 16^+ of the band 1 in ^{144}Tb, five new coincident γ-ray transitions of 222.7, 273.9, 411.9, 806.5, and 1255.6 keV are observed in the γ-ray spectra. The present DCO analyses suggest stretched dipole natures for the 222.7, 273.9, and 411.9 keV transitions and a stretched quadrupole character for the 1255.6 keV transition. Based on the DCO ratio analyses and coincident relationships, band 3 is first constructed in the present work.

III. DISCUSSION

The low-lying structure in ^{144}Tb has been well described with the spherical shell model and the three lowest states 9^+, 10^+, and 11^+ in band 1 have been considered as the multiplets of the $\pi h_{11/2} \otimes \nu h_{11/2}^{-1}$ configuration [4,11]. However, the irregular high-spin states of band 1 above ~1.8 MeV could not be reproduced by the shell model calculations within only the $\pi(h_{11/2})^1 \otimes \nu(d_{3/2}s_{1/2}h_{11/2})^{-3}$ model space [11], which implied that these high-spin states in ^{144}Tb may involve more complex multi-particle-hole configurations. In Fig. 4, the excitation energies of the 12^+ and 14^+ states relative to the 10^+ level in $N = 79$ ^{142}Eu and ^{144}Tb isotones are compared with those of the 2^+ and 4^+ states relative to the 0^+ ground

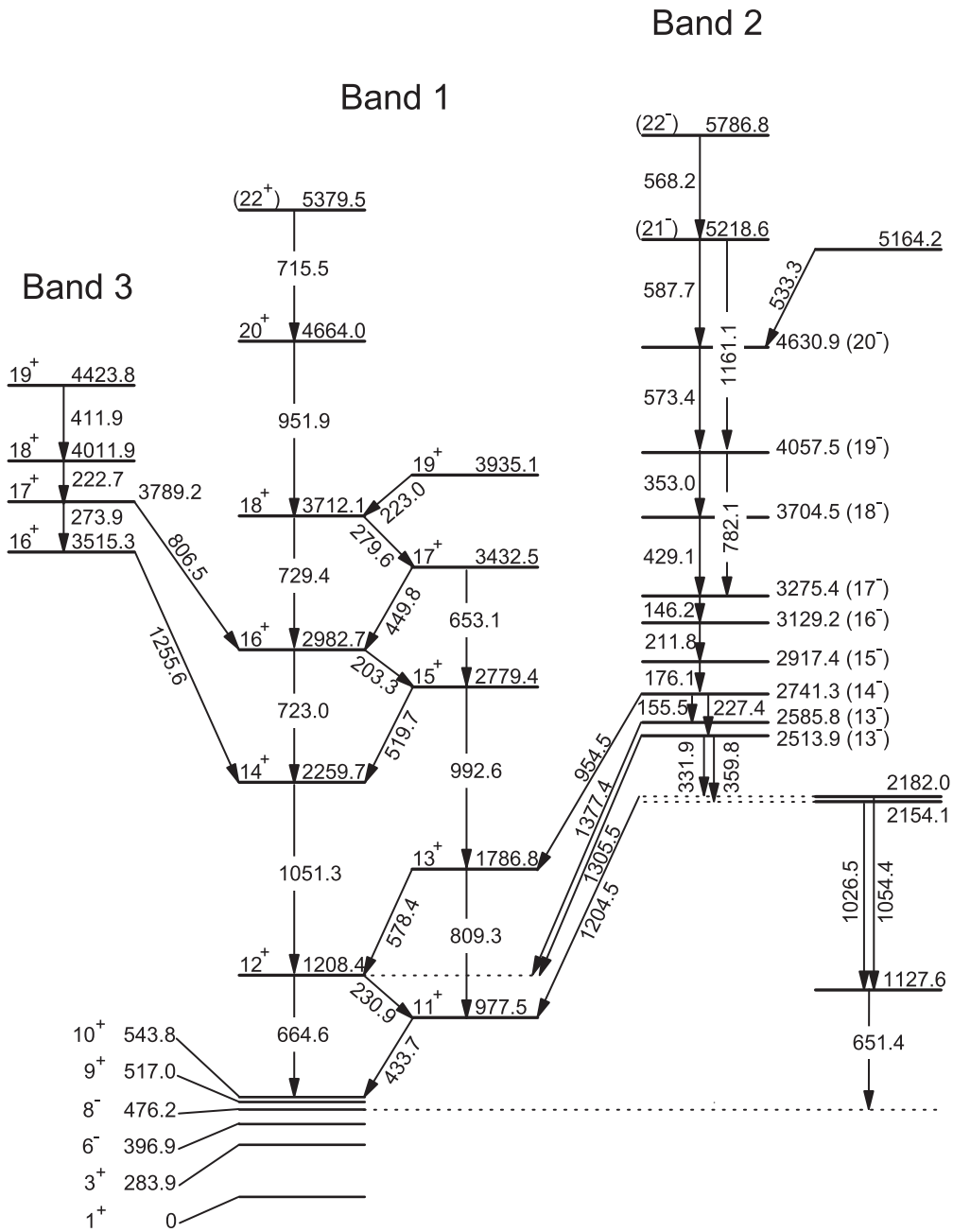

FIG. 3. Partial level scheme of ^{144}Tb. Apart from the levels below 10^+, all the levels shown have been identified in the present work. Energies are in keV.

state in $N = 80$ ^{142}Sm and ^{144}Gd cores, respectively. These 2^+ and 4^+ states in ^{142}Sm and ^{144}Gd have been interpreted as neutron excitations and predominantly formed by two neutron holes in the lower $s_{1/2}$, $d_{3/2}$, $g_{7/2}$, and $d_{5/2}$ orbitals [20]. In Ref. [3], the states 12^+ and 14^+ in ^{142}Eu have been explained as ^{142}Sm core excitations. Here, the remarkable similarity of excitation energies between ^{144}Tb and ^{144}Gd indicates that the 12^+ and 14^+ states in band 1 of ^{144}Tb can also be explained in terms of the coupling of an $h_{11/2}$ proton particle and an $h_{11/2}$ neutron hole to the 2^+ and 4^+ excited states in the doubly even ^{144}Gd core. Above the spin 14^+ in ^{144}Tb, a coupling structure is observed in band 1. A similar structure has also been found in ^{142}Eu [10]. Since several competing configurations are probably associated with these high-lying structures in ^{142}Eu [10] and also in ^{144}Tb, more studies are needed to clarify the nature of this structure.

The dipole band 3 with bandhead of 16^+ is newly observed in this work. In the neighboring odd-A and odd-odd $N = 79$ isotones, the dipole bands with bandhead of $23/2^-$ level and 16^+ level, respectively, have been observed [10,14,21–24]. Since the $Z = 64$ proton subshell closure is much weaker than the $N = 82$ neutron shell closure, the $\pi h_{11/2}^2$ configuration from the proton excitation across the $Z = 64$ gap will play an important role [21,22,25,26]. In Refs. [14,21,22], the

TABLE I. γ-ray energies, excitation energies, relative γ-ray intensities, and DCO ratios in ^{144}Tb.

E_γ (keV)[a]	E_i (keV)	E_f (keV)	Intensity (%)	DCO ratio	Assignment
146.2	3275.4	3129.2	23.5(44)	0.29(5)	$(17^-) \rightarrow (16^-)$
155.5	2741.3	2585.8	3.6(8)		$(14^-) \rightarrow (13^-)$
176.1	2917.4	2741.3	32.9(58)	1.04(12)	$(15^-) \rightarrow (14^-)$
203.3	2982.7	2779.4	20.6(32)	0.46(8)	$16^+ \rightarrow 15^+$
211.8	3129.2	2917.4	28.7(54)	1.13(31)	$(16^-) \rightarrow (15^-)$
222.7	4011.9	3789.2	3.1(6)	0.56(8)[b]	$18^+ \rightarrow 17^+$
223.0	3935.1	3712.1	11.9(33)	0.56(8)[b]	$19^+ \rightarrow 18^+$
227.4	2741.3	2513.9	14.7(32)		$(14^-) \rightarrow (13^-)$
230.9	1208.4	977.5	46.5(65)	0.71(14)	$12^+ \rightarrow 11^+$
273.9	3789.2	3515.3	5.1(8)	0.68(13)	$17^+ \rightarrow 16^+$
279.6	3712.1	3432.5	11.1(16)	0.79(12)	$18^+ \rightarrow 17^+$
331.9	2513.9	2182.0	2.2(6)		
353.0	4057.5	3704.5	14.4(27)	0.56(6)	$(19^-) \rightarrow (18^-)$
359.8	2513.9	2154.1			
411.9	4423.8	4011.9	7.9(14)	0.37(6)	$19^+ \rightarrow 18^+$
429.1	3704.5	3275.4	26.0(39)	0.37(3)	$(18^-) \rightarrow (17^-)$
433.7	977.5	543.8	89.6(100)	0.50(10)	$11^+ \rightarrow 10^+$
449.8	3432.5	2982.7	13.5(22)	0.32(5)	$17^+ \rightarrow 16^+$
519.7	2779.4	2259.7	26.9(40)	0.41(8)	$15^+ \rightarrow 14^+$
533.3	5164.2	4630.9			
568.2	5786.8	5218.6	3.7(8)		
573.4	4630.9	4057.5	8.0(16)		$(20^-) \rightarrow (19^-)$
578.4	1786.8	1208.4	54.9(86)	0.52(9)	$13^+ \rightarrow 12^+$
587.7	5218.6	4630.9	4.8(9)		$(21^-) \rightarrow (20^-)$
651.4	1127.6	476.2			
653.1	3432.5	2779.4	4.1(8)		$17^+ \rightarrow 15^+$
664.6	1208.4	543.8	100	0.96(16)	$12^+ \rightarrow 10^+$
715.5	5379.5	4664.0	5.2(15)		$(22^+) \rightarrow 20^+$
723.0	2982.7	2259.7	12.9(27)	1.58(22)	$16^+ \rightarrow 14^+$
729.4	3712.1	2982.7	16.4(25)	1.06(12)	$18^+ \rightarrow 16^+$
782.1	4057.5	3275.4	6.0(11)		$(19^-) \rightarrow (17^-)$
806.5	3789.2	2982.7	3.4(6)	0.47(14)	$17^+ \rightarrow 16^+$
809.3	1786.8	977.5	9.4(19)		$13^+ \rightarrow 11^+$
951.9	4664.0	3712.1	12.7(33)	0.96(14)	$20^+ \rightarrow 18^+$
954.5	2741.3	1786.8	26.5(50)	0.81(27)	$(14^-) \rightarrow 13^+$
992.6	2779.4	1786.8	22.7(36)	1.12(30)	$15^+ \rightarrow 13^+$
1026.5	2154.1	1127.6			
1051.3	2259.7	1208.4	60.1(93)	1.06(23)	$14^+ \rightarrow 12^+$
1054.4	2182.0	1127.6			
1161.1	5218.6	4057.5	2.7(8)		$(21^-) \rightarrow (19^-)$
1204.5	2182.0	977.5			
1255.6	3515.3	2259.7	10.9(32)	1.14(23)	$16^+ \rightarrow 14^+$
1305.5	2513.9	1208.4	15.8(31)	0.59(9)	$(13^-) \rightarrow 12^+$
1377.4	2585.8	1208.4	7.3(14)		$(13^-) \rightarrow 12^+$

[a]Uncertainties between 0.1 and 0.5 keV.

[b]DCO ratio is for total peak.

$\pi h_{11/2}^2 \otimes \nu h_{11/2}^{-1}$ configuration has been assigned to these dipole bands in odd-A ^{141}Sm,^{143}Gd, and ^{145}Dy isotones. In Fig. 5, the angular momenta as functions of the rotational frequency for the dipole bands in the $N = 79$ isotones are plotted. It can be clearly seen that the experimental $I \sim \hbar\omega$ relations are very close to each other for the odd-A isotones, both in the magnitude and in the slope. The angular momenta of the dipole bands in odd-odd isotones also have frequency dependences similar to those in the odd-A isotones. At a given rotational frequency, the angular momentum for an odd-odd isotone is approximately $4\hbar$ larger than that of an odd-A isotone. This indicates that the angular momentum contribution of the additional valence proton in odd-odd isotones may come from the $h_{11/2}$ orbital. Therefore, the $\pi h_{11/2}^3 \otimes \nu h_{11/2}^{-1}$ configuration is assigned to the dipole bands in the odd-odd $N = 79$ isotones.

With the newly observed dipole band in ^{144}Tb and the similar dipole bands known previously in the neighboring

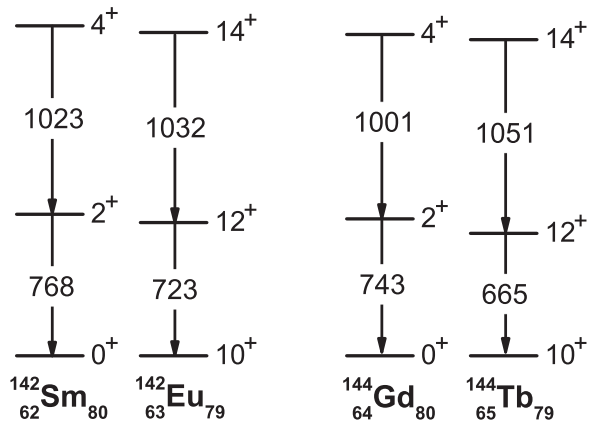

FIG. 4. Comparison between the 12^+, 14^+ states in ^{142}Eu, ^{144}Tb, and the 2^+, 4^+ states in the $N = 80$ ^{142}Sm, ^{144}Gd cores, respectively. The experimental data are taken from Refs. [10,20].

$N = 79$ isotones, it is therefore very interesting to perform a systematic investigation of these dipole bands and probe their structure evolution with the proton number across the $Z = 64$ subshell. Theoretically, the tilted-axis-cranking (TAC) model [27] has been widely used to describe the properties of the dipole bands in the weakly deformed nuclei. In particular, the TAC model based on the covariant density functional theory (CDFT) [28–30] has attracted much attention recently [31]; therein, the density functional has either the meson exchange [32,33] or the point-coupling form [34]. So far, the TAC-CDFT has been well applied to study magnetic dipole bands in mass regions $A \sim 60$ [34,35], 80 [32,36], 100 [37,38], 140 [33], and 200 [39], as well as antimagnetic rotational bands in ^{105}Cd [40,41] and ^{112}In [42]. In the present work, the self-consistent TAC-CDFT based on the point-coupling density functional PC-PK1 [43] is applied to investigate the dipole bands in ^{144}Tb and neighboring $N = 79$ isotones. In the present calculations, the high-j nucleon configuration is fixed to $\pi h_{11/2}^2 \otimes \nu h_{11/2}^{-1}$ for odd-A isotones and $\pi h_{11/2}^3 \otimes \nu h_{11/2}^{-1}$ for odd-odd ones, i.e., the unpaired valence proton particles are fixed to occupy the two or three $h_{11/2}$ orbits, and a valence neutron hole is fixed to occupy the $h_{11/2}$ orbit. The Dirac equation for the nucleons is solved in a three-dimensional Cartesian harmonic-oscillator basis with ten major shells, and the pairing correlations are neglected.

In Fig. 6, the calculated energy spectrum by TAC-CDFT is compared with the experimental data for band 3 in ^{144}Tb. The experimental excitation energies are well reproduced by the TAC-CDFT calculations. In Fig. 5, the angular momenta as functions of the rotational frequency from the TAC-CDFT calculations for the dipole bands in the $N = 79$ isotones are compared with the experimental data. Good agreement is also obtained for ^{144}Tb. The remarkable agreement between the calculated results and the experimental data for ^{144}Tb further supports the $\pi h_{11/2}^3 \otimes \nu h_{11/2}^{-1}$ configuration assignment for band 3 of ^{144}Tb.

As shown in Fig. 5, in general the theoretical results can reproduce the $I \sim \hbar\omega$ relations for both the odd-A and odd-odd isotones. A $\sim 2\hbar$ overestimate found in dipole bands of ^{141}Sm and ^{142}Eu, as well as the relatively rapid increase in dipole bands of ^{143}Gd and ^{144}Tb, can be ascribed to the

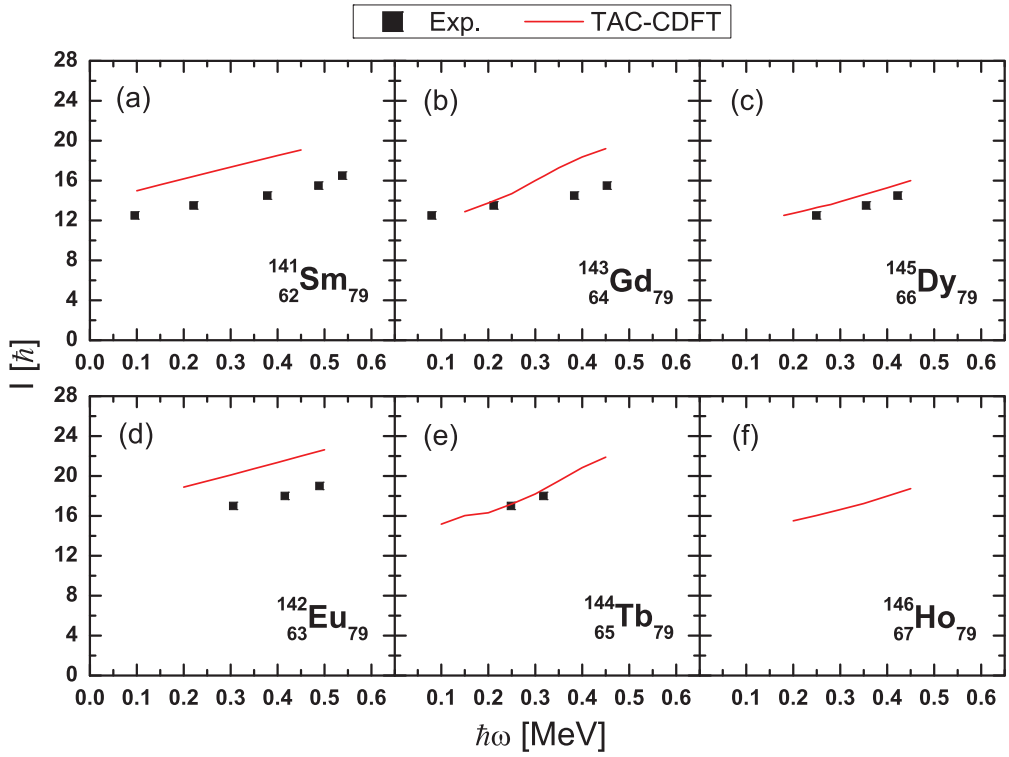

FIG. 5. (Color online) The experimental and calculated angular momenta as functions of the rotational frequency for the dipole bands in the $N = 79$ isotones. The experimental data are taken from Refs. [10,14,22–24].

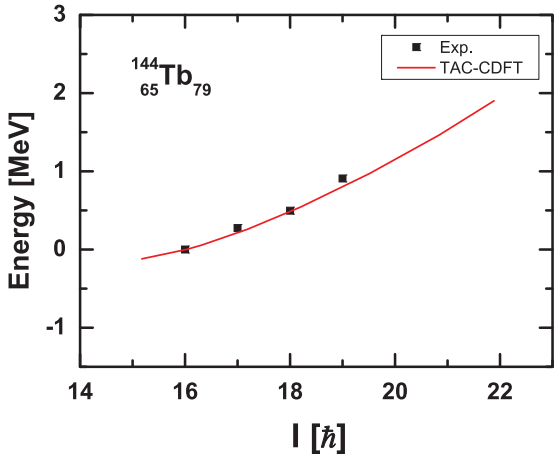

FIG. 6. (Color online) The calculated energy spectrum of band 3 in ^{144}Tb by TAC-CDFT in comparison with the experimental data. The energy at $I = 16\hbar$ is taken as the reference of comparison.

neglecting of pairing correlations in the present calculations. The inclusion of pairing is expected to reduce the moment of inertia and lower the spin at a fixed frequency. For these $N = 79$ isotones, due to the blocking effect of the valence $\pi h_{11/2}$ particles and $\nu h_{11/2}$ hole, the pairing correlations have been largely reduced for the negative-parity orbitals. Meanwhile, due to the sparse positive-parity neutron orbitals near the Fermi surface, the positive-parity neutron orbitals also contribute little to pairing correlations. In contrast, the pairing correlations could play an important role for the positive-parity proton orbitals in these $N = 79$ isotones discussed here. Regarding the existence of the subshell $Z = 64$, for these discussed dipole bands, the effect of pairing correlations should be more important for the positive-parity proton orbitals of Sm and Eu (four proton holes in $Z = 64$ subshell closure) than those of Dy and Ho (zero proton holes).

Here, to address the angular momentum contribution of positive-parity proton orbitals, we provide Table II, where the contributions of the positive-parity proton orbitals to the angular momentum component along the long axis j_3 are listed. It is obvious that the values of ^{141}Sm and ^{142}Eu are $\sim 3\hbar$ larger than those of ^{145}Dy and ^{146}Ho. The values of ^{143}Gd and ^{144}Tb are close to the latter at low rotational frequency, and increase rapidly with increasing rotational frequency. Therefore, the contributions from the low-j positive-parity proton levels are mainly responsible for the overestimate of the $I \sim \hbar\omega$ relations in dipole bands of ^{141}Sm and ^{142}Eu and the rapid increase of those of ^{143}Gd and ^{144}Tb. As the pairing correlations always tend to hinder the angular momentum alignment of nucleons, the inclusion of pairing correlations will certainly decrease the calculated values of the total angular momentum, and give a better description of the $I \sim \hbar\omega$ relations for these $N = 79$ isotones. Unfortunately, this is not easy, and the implementation of TAC-CDFT with pairing correlations is still ongoing.

TABLE II. Contribution of the positive-parity proton orbitals to the angular momentum component along the long axis j_3 in the N=79 isotones calculated with the TAC-CDFT without the pairing correlations. (in units of $\hbar$)

$\hbar\omega$ (MeV)	^{141}Sm	^{142}Eu	^{143}Gd	^{144}Tb	^{145}Dy	^{146}Ho
0.2	4.02	3.95	1.85	1.23	1.11	0.93
0.3	4.32	4.29	3.83	3.44	1.78	1.62
0.4	4.57	4.55	5.65	5.44	2.61	2.43

In Fig. 7, the evolutions of deformation parameters β and γ driven by increasing rotational frequency in the TAC-CDFT calculations are presented for the dipole bands in $N = 79$ isotones. As shown in Fig. 7, the β value is around 0.15 in all the discussed $N = 79$ isotones, which indicates a relatively small quadrupole deformation and is typical in the $A \sim 140$ mass region. The γ values change very slightly with increasing rotational frequency from 0.2 to 0.45 MeV. As the proton number increases, a shape evolution from a triaxial deformation ($\gamma \sim 35^\circ$) in ^{141}Sm and ^{142}Eu to a nearly oblate deformation ($\gamma \sim 55^\circ$) in ^{145}Dy and ^{145}Ho is predicted. Since the valence nucleon number on high-j $h_{11/2}$ orbits has been fixed for the discussed $N = 79$ isotones, the shape evolution might be caused by the gradual occupation of the gd shell below the $Z = 64$ energy gap as the proton number increases.

As the dipole band observed in ^{143}Gd has been suggested to be magnetic rotational band [14], the dipole bands in the neighboring $N = 79$ isotones might be also considered magnetic rotational bands due to the similar structures. In order to investigate the possible magnetic rotational nature of these dipole bands in the $N = 79$ isotones, here the shears mechanism is examined in Fig. 8 from the composition of the total angular momentum in TAC-CDFT calculations. The proton and neutron angular momentum vectors $\boldsymbol{J}_\pi$ and $\boldsymbol{J}_\nu$ as well as the total angular momentum vector $\boldsymbol{J}_{\rm tot} = \boldsymbol{J}_\pi + \boldsymbol{J}_\nu$ at both a low $\hbar\omega = 0.2$ MeV and a high $\hbar\omega = 0.4$ MeV rotational frequency are shown in the figure. Here, the $\boldsymbol{J}_\pi$ and $\boldsymbol{J}_\nu$ are defined as

$$\boldsymbol{J}_\pi = \langle \hat{\boldsymbol{J}}_\pi \rangle = \sum_{p=1}^{Z} \langle p|\hat{J}|p\rangle, \quad \boldsymbol{J}_\nu = \langle \hat{\boldsymbol{J}}_\nu \rangle = \sum_{n=1}^{N} \langle n|\hat{J}|n\rangle,$$

where the sum runs over all the proton (or neutron) orbitals occupied in the cranking wave function in the intrinsic system. In TAC-CDFT calculations, both angular momentum components along the short and the long principal axes of nuclear density distribution can be obtained.

For two or more quasiparticle excited bands, it is well known that, regardless of the core polarization, the contributions to the angular momentum come mainly from the valence particles and holes, especially for the levels near bandhead. Taking ^{141}Sm with the configuration $\pi h_{11/2}^2 \otimes \nu h_{11/2}^{-1}$ as an example, as shown in Fig. 8, at the low rotational frequency $\hbar\omega = 0.2$ MeV, the valence proton particles filling the bottom of the $h_{11/2}$ shell contribute mainly to the proton angular momentum along the short axis, and the valence neutron hole at the upper end of $h_{11/2}$ shell contributes mainly to the neutron angular momentum along the long axis. They form the two blades of the shears. As the frequency increases, the two blades move toward each other while keeping the direction of the total angular momentum with nearly constant tilted angle.

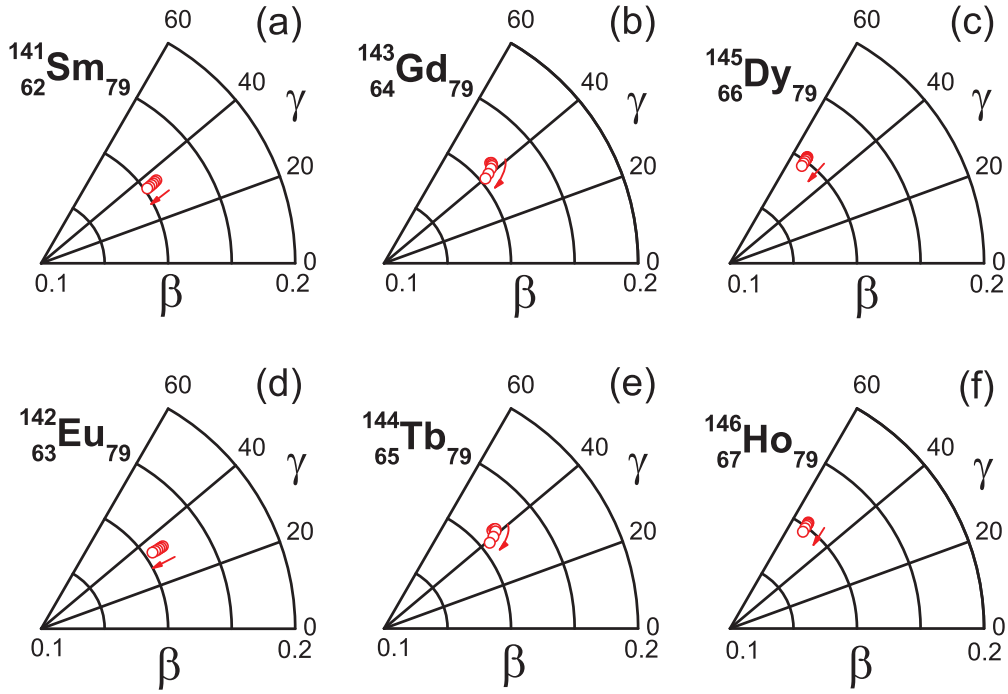

FIG. 7. (Color online) Evolutions of deformation parameters β and γ driven by increasing rotational frequency in the TAC-CDFT calculations for the dipole bands in the $N = 79$ isotones. The arrows indicate the increasing direction of rotational frequency $\hbar\omega$, which changes from 0.2 to 0.45 MeV in all the cases. The γ axes are in units of degrees.

In such a way, the shears mechanism can be clearly seen. Similar shears mechanisms can also be found for the dipole bands with configuration $\pi h_{11/2}^{2} \otimes \nu h_{11/2}^{-1}$ in odd-A isotones ^{143}Gd and ^{145}Dy, as well as the dipole bands with configuration $\pi h_{11/2}^{3} \otimes \nu h_{11/2}^{-1}$ in odd-odd isotones ^{142}Eu, ^{144}Tb, and ^{146}Ho. It should be noted that, as seen in Fig. 8, with the increase of $\hbar\omega$, in some cases the component of proton angular momentum along the long axis increases a lot and then the tilted angles of the total angular momentum have an obvious change. This effect just corresponds to the rapid increase of the contribution

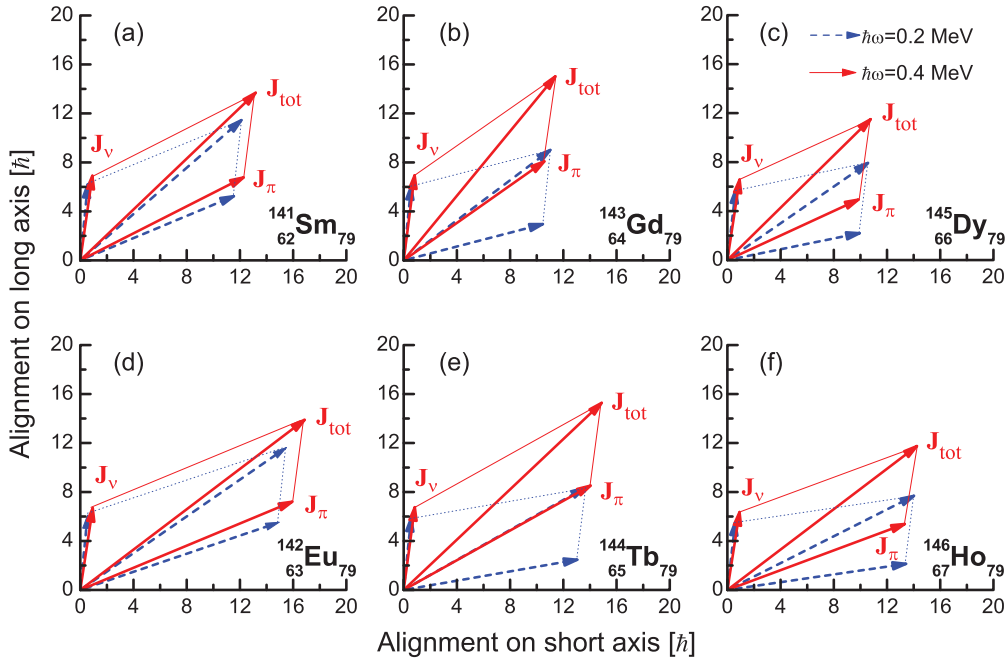

FIG. 8. (Color online) Composition of the total angular momentum at rotational frequencies $\hbar\omega = 0.2$ and 0.4 MeV in TAC-CDFT calculations for magnetic rotational bands in the $N = 79$ isotones.

of positive-parity proton orbitals (gd shell) to the angular momentum component along the long axis, as presented in Table II. The inclusion of pairing correlations will reduce this contribution of positive-parity proton orbitals, and will lead to a better realization of the shears mechanism.

IV. SUMMARY

The spectroscopy of ^{144}Tb has been studied via ^{116}Sn(^{32}S, $3n1p$)^{144}Tb fusion-evaporation reaction at a beam energy of 156 MeV. A dipole band, which is suggested to be built on the $\pi h_{11/2}^{3} \otimes \nu h_{11/2}^{-1}$ configuration, is observed for the first time. The properties of dipole bands in $N = 79$ isotones are discussed in terms of the self-consistent tilted-axis-cranking covariant density functional theory (TAC-CDFT). In addition, the shears mechanism of these dipole bands in the $N = 79$ isotones is examined to investigate the magnetic rotational nature. Based on systematic comparisons and analyses, the newly observed dipole band in ^{144}Tb can be interpreted as a magnetic rotational band.

ACKNOWLEDGMENTS

This work is support by the Natural Science Foundation of China under Grants No. 11175003, No. 11235001, No. 11335002, No. 11320101004, No. 11375017, No. 11375015, No. 11345004, No. 11175002, and No. J1103206 and the Chinese Major State Basic Research Development Program under Grant No. 2013CB834400. The authors wish to thank Dr. Q. W. Fan for making the target, and the staffs in the tandem accelerator laboratory at the China Institute of Atomic Energy (CIAE), Beijing.

[1] M. A. Rizzutto, E. W. Cybulska, V. R. Vanin, J. R. B. Oliveira, L. G. R. Emediato, R. V. Ribas, W. A. Seale, M. N. Rao, N. H. Medina, S. Botelho, J. C. Aequadro, and C. L. Lima, Z. Phys. A **344**, 221 (1992).
[2] G. de Angelis, S. Lunardi, D. Bazzacco, J. Rico, F. Terrasi, M. Piiparinen, A. Atac, and J. Nyberg, Z. Phys. A **347**, 93 (1993).
[3] A. M. Bizzeti-Sona, P. G. Bizzeti, F. Banci Buonamici, D. Bazzacco, S. Lunardi, F. Soramel, G. Lo Bianco, N. Molho, G. De Angelis, and J. Simpson, Z. Phys. A **337**, 235 (1990).
[4] M. Sferrazza, D. Bazzacco, S. Lunardi, E. Maglione, M. A. Cardona, G. de Angelis, J. Rico, A. Facco, P. G. Bizzeti, and A. M. Bizzeti-Sona, Z. Phys. A **344**, 123 (1992).
[5] A. A. Sonzogni, Nucl. Data Sheets **98**, 515 (2003).
[6] L. K. Peker, Nucl. Data Sheets **51**, 395 (1987).
[7] L. K. Peker, Nucl. Data Sheets **43**, 579 (1984).
[8] M. L. Li, S. J. Zhu, X. L. Che, Y. N. Yu, Y. J. Chen, H. B. Ding, L. H. Zhu, X. G. Wu, S. X. Wen, C. Y. He, X. Z. Cui, and Y. Liu, Phys. Rev. C **75**, 034304 (2007).
[9] J. G. Wang, S. J. Zhu, L. Gu, Z. G. Xiao, E. Y. Yeoh, M. Zhang, Y. Liu, H. B. Ding, Q. Xu, L. H. Zhu, X. G. Wu, Y. S. Chen, C. Y. He, G. S. Li, L. L. Wang, Y. Zhang, and B. Zhang, J. Phys. G: Nucl. Part. Phys. **37**, 125107 (2010).
[10] M. Piiparinen, A. Ataç, J. Blomqvist, G. B. Hagemann, B. Herskind, R. Julin, S. Juutinen, A. Lampinen, J. Nyberg, G. Sletten, P. Tikkanen, S. Törmänen, A. Virtanen, and R. Wyss, Nucl. Phys. A **605**, 191 (1996).
[11] M. Sferrazza, M. A. Cardona, D. Bazzacco, S. Lunardi, E. Maglione, and G. de Angelis, Z. Phys. A **354**, 157 (1996).
[12] S. Frauendorf, Rev. Mod. Phys. **73**, 463 (2001).
[13] F. Brandolini, M. Ionescu-Bujor, N. H. Medina, R. V. Ribas, D. Bazzacco, M. De Poli, P. Pavan, C. Rossi Alvarez, G. de Angelis, S. Lunardi, D. De Acuña, D. R. Napoli, and S. Frauendorf, Phys. Lett. B **388**, 468 (1996).
[14] T. Rząca-Urban, Acta Phys. Pol. B **32**, 2645 (2001).
[15] R. M. Lieder, T. Rząca-Urban, H. Brands, W. Gast, H. M. Jäger, L. Mihailescu, Z. Marcinkowska, W. Urban, T. Morek, Ch. Droste, P. Szymański, S. Chmel, D. Bazzacco, G. Falconi, R. Menegazzo, S. Lunardi, C. Rossi Alvarez, G. de Angelis, E. Farnea, A. Gadea, D. R. Napoli, Z. Podolyak, Ts. Venkova, and R. Wyss, Eur. Phys. J. A **13**, 297 (2002).
[16] E. O. Podsvirova, R. M. Lieder, A. A. Pasternak, S. Chmel, W. Gast, Ts. Venkova, H. M. Jäger, L. Mihailescu, G. de Angelis, D. R. Napoli, A. Gadea, D. Bazzacco, R. Menegazzo, S. Lunardi, W. Urban, Ch. Droste, T. Morek, T. Rząca-Urban, and G. Duchêne, Eur. Phys. J. A **21**, 1 (2004).
[17] Krishichayan, A. Chakraborty, S. S. Ghugre, R. Goswami, S. Mukhopadhyay, N. S. Pattabiraman, S. Ray, A. K. Sinha, S. Sarkar, P. V. Madhusudhana Rao, U. Garg, S. K. Basu, B. K. Yogi, L. Chaturvedi, A. Dhal, R. K. Sinha, M. Saha Sarkar, S. Saha, R. Singh, R. K. Bhowmik, A. Jhingan, N. Madhavan, S. Muralithar, S. Nath, R. P. Singh, and P. Sugathan, Phys. Rev. C **70**, 044315 (2004).
[18] M. Sugawara, Y. Toh, M. Oshima, M. Koizumi, A. Osa, A. Kimura, Y. Hatsukawa, J. Goto, H. Kusakari, T. Morikawa, Y. H. Zhang, X. H. Zhou, Y. X. Guo, and M. L. Liu, Phys. Rev. C **79**, 064321 (2009).
[19] D. C. Radford, Nucl. Instrum. Methods Phys. Res. Sect. A **361**, 297 (1995).
[20] M. Lach, J. Styczen, R. Julin, M. Piiparinen, H. Beuscher, P. Kleinheinz, and J. Blomqvist, Z. Phys. A **319**, 235 (1984).
[21] M. A. Cardona, G. de Angelis, D. Bazzacco, M. De Poli, and S. Lunardi, Z. Phys. A **340**, 345 (1991).
[22] M. Sferrazza, M. A. Cardona, G. de Angelis, D. Bazzacco, and S. Lunardi, Z. Phys. A **350**, 5 (1994).
[23] M. Lach, P. Kleinheinz, J. Blomqvist, A. Ercan, H. J. Hähn, D. Wahner, R. Julin, M. Zupancic, F. Cigoroglu, and G. de Angelis, Z. Phys. A **345**, 427 (1993).
[24] M. Sugawara, H. Kusakari, Y. Igari, K. Myojin, D. Nishimiya, S. Mitarai, M. Oshima, T. Hayakawa, M. Kidera, K. Furutaka, and Y. Hatsukawa, Eur. Phys. J. A **1**, 123 (1998).
[25] H. A. Roth, S. E. Arnell, D. Foltescu, Ö. Skeppstedt, J. Blomqvist, G. de Angelis, D. Bazzacco, and S. Lunardi, Eur. Phys. J. A **10**, 275 (2001).
[26] P. Kleinheinz, R. Broda, P. J. Daly, S. Lunardi, M. Ogawa, and J. Blomqvist, Z. Phys. A **290**, 279 (1979).
[27] S. Frauendorf, Nucl. Phys. A **557**, 259 (1993).
[28] P. Ring, Prog. Part. Nucl. Phys. **37**, 193 (1996).
[29] D. Vretenar, A. V. Afanasjev, G. A. Lalazissis, and P. Ring, Phys. Rep. **409**, 101 (2005).
[30] J. Meng, H. Toki, S. G. Zhou, S. Q. Zhang, W. H. Long, and L. S. Geng, Prog. Part. Nucl. Phys. **57**, 470 (2006).

[31] J. Meng, J. Peng, S. Q. Zhang, and P. W. Zhao, Front. Phys. **8** (1), 55 (2013).
[32] H. Madokoro, J. Meng, M. Matsuzaki, and S. Yamaji, Phys. Rev. C **62**, 061301 (2000).
[33] J. Peng, J. Meng, P. Ring, and S. Q. Zhang, Phys. Rev. C **78**, 024313 (2008).
[34] P. W. Zhao, S. Q. Zhang, J. Peng, H. Z. Liang, P. Ring, and J. Meng, Phys. Lett. B **699**, 181 (2011).
[35] D. Steppenbeck, R. V. F. Janssens, S. J. Freeman, M. P. Carpenter, P. Chowdhury, A. N. Deacon, M. Honma, H. Jin, T. Lauritsen, C. J. Lister, J. Meng, J. Peng, D. Seweryniak, J. F. Smith, Y. Sun, S. L. Tabor, B. J. Varley, Y. C. Yang, S. Q. Zhang, P. W. Zhao, and S. Zhu, Phys. Rev. C **85**, 044316 (2012).
[36] J. Li, C. Y. He, Y. Zheng, C. B. Li, K. Y. Ma, and J. B. Lu, Phys. Rev. C **88**, 014317 (2013).
[37] C. B. Li, J. Li, X. G. Wu, X. F. Li, Y. Zheng, C. Y. He, G. S. Li, S. H. Yao, B. B. Yu, X. P. Cao, S. P. Hu, J. L. Wang, C. Xu, and Y. Y. Cheng, Nucl. Phys. A **892**, 34 (2012).
[38] K. Y. Ma, J. B. Lu, D. Yang, H. D. Wang, Y. Z. Liu, J. Li, L. H. Zhu, X. G. Wu, Y. Zheng, and C. Y. He, Eur. Phys. J. A **48**, 82 (2012).
[39] L. F. Yu, P. W. Zhao, S. Q. Zhang, P. Ring, and J. Meng, Phys. Rev. C **85**, 024318 (2012).
[40] P. W. Zhao, J. Peng, H. Z. Liang, P. Ring, and J. Meng, Phys. Rev. Lett. **107**, 122501 (2011).
[41] P. W. Zhao, J. Peng, H. Z. Liang, P. Ring, and J. Meng, Phys. Rev. C **85**, 054310 (2012).
[42] X. W. Li, J. Li, J. B. Lu, K. Y. Ma, Y. H. Wu, L. H. Zhu, C. Y. He, X. Q. Li, Y. Zheng, G. S. Li, X. G. Wu, Y. J. Ma, and Y. Z. Liu, Phys. Rev. C **86**, 057305 (2012).
[43] P. W. Zhao, Z. P. Li, J. M. Yao, and J. Meng, Phys. Rev. C **82**, 054319 (2010).